DOI 10.1007/s11182-021-02303-8
Russian Physics Journal, Vol. 64, No. 1, May, 2021 (Russian Original No. 1, January, 2021)

STRUCTURE, PHASE COMPOSITION AND PROPERTIES OF RAIL RUNNING SURFACE AT EXTREMELY LONG OPERATION TIME

Yu. F. Ivanov,[1] V. E. Kormyshev,[2] V. E. Gromov,[2] and A. A. Yur'ev[3]

UDC 669.539.382:669.17

The paper presents investigations of the structure, phase composition and properties of the rail running after bulk steel hardening. Investigations are performed at a different depth by using modern techniques of material physics in extremely long operation conditions (gross weight of 1411 million tons). The Rockwell hardness measurements at a depth ranging from 2 to 10 mm, show a decrease in the hardness level from 37.1 to 35.8 HRC and in the microhardness – from 1481 to 1210 MPa, respectively. The multiple modifications of the rail running surface include the disintegration of lamellar perlite and the formation of the submicron size subgrain structure varying between 100 and 150 nm; the formation of 30–55 nm carbide phase nanoparticles on the grain boundaries and in the subgrain volume; the growth in microdistortions and the crystal lattice parameter of the α-Fe solid solution; the increase in the scalar dislocation density. Possible reasons of these changes are discussed herein.

Keywords: rail running surface, structure, properties, dislocation, operation.

INTRODUCTION

The formation and evolution of the structure, phase composition and properties of the rail running surface during long-term operation represent several interrelated scientific and technical issues. On the one hand, it is a deep understanding of the fundamental problems of condensed matter physics, and on the other, its practical significance [1].

In 2013, AO "Evraz West-Siberian Metal Plant" (Novokuznetsk, Russia) began the production of hundred-meter rails hardened by air jet in rolling mill machines. A certified batch of rails was installed for the experimental circle railway in Shcherbinka town with the train traffic with the gross weight of 1700 million tons by now.

There is virtually no information offered in the literature concerning the evolution of the structure, phase composition and properties of the rail running surface after the train traffic with the gross weight over 1000 million tons [1]. Nevertheless, the literature review [2–8] shows that already at the gross weight not over 300 million tons, the rail running surface structure starts to modify, i.e., the microhardness becomes anomalously high and the cementite fracture occurs. During a long-term operation, multiple defects accumulate in rails, and segregation, relaxation, homogenization and recrystallization processes and phase transformations occur, that cause a deterioration of physical and mechanical properties of rails resulting in their breakdown.

The main parameters of the structure, phase composition and defect substructure formation and evolution were determined for bulk-hardened rails at a different depth in the rail head surface after the train traffic with a weight of 500 and 1000 million tons [1, 9, 10]. In works [11, 12], these dependences were obtained only after the train traffic with the gross rail load of 692 million tons for bulk-hardened, long-length hundred-meter rails, which are still being tested.

[1]Institute of High Current Electronics of the Siberian Branch of the Russian Academy of Sciences, Tomsk, Russia, e-mail: yufi55@mail.ru; [2]Siberian State Industrial University, Novokuznetsk, Russia, e-mail: gromov@physics.sibsiu.ru; gromov@physics.sibsiu.ru; [3]AO "Evraz West-Siberian Metal Plant", Novokuznetsk, Russia, e-mail: ant-yurev@yandex.ru. Translated from Izvestiya Vysshikh Uchebnykh Zavedenii, Fizika, No. 1, pp. 71–77, January, 2021. Original article submitted April 16, 2020; revision submitted June 29, 2020.

TABLE 1. Chemical Composition of DT350 Category Rails

Analysis	Chemical composition, wt.%										
	C	Mn	Si	P	S	Cr	Ni	Cu	V	Al	Ti
Checkup analysis	0.72	0.77	0.61	0.010	0.009	0.42	0.07	0.14	0.038	0.003	0.003
Russian rail steel specifications	0.71–0.82	0.75–1.25	0.25–0.60	Not over		0.20–0.80	Σ not over 0.27%		0.03–0.15	Not over	
				0.020	0.020		0.20	0.20		0.004	0.025

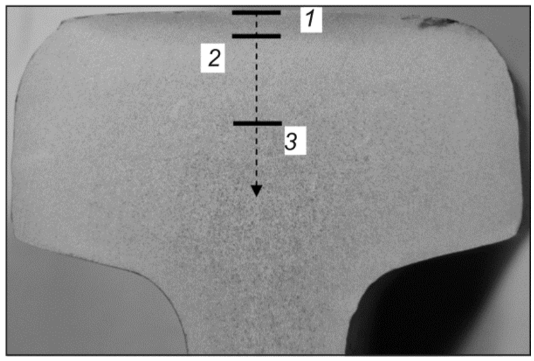

Fig. 1. Rail head and schematic of the film preparation: *1* – rail running surface, *2* – 2 mm depth layer, *3* – 10 mm depth layer.

The aim of this work is to identify the regularities and carry out a comparative analysis of the structure, phase composition, defect substructure and properties developing at a different depth on the central axis of the rail head of bulk-hardened, hundred-meter rails after the extremely long operation time.

MATERIALS AND METHODS

For this experiment, the category DT350 rails made of rail steel, were removed from the experimental circle track in Shcherbinka after the train traffic with the gross rail load of 1411 million tons. In 2013, the certified batch of rails was manufactured in AO “Evraz West-Siberian Metal Plant” (Novokuznetsk, Russia) in accordance with the Russian specifications and then subjected to bulk hardening. The chemical composition given in Table 1 for the DT350 category rails satisfied these specifications.

The steel macrostructure was studied after chemical etching in a hot 50% HCl solution on an incomplete transverse template (rail head or web). The steel macrostructure was analyzed in accordance with the Russian Detailed Design Document “Classifier of macrostructure defects in rails produced from continuous cast steel billets”. The steel microstructure was investigated on microsections cut from the upper part of the rail head after chemical etching in a 4% solution of nitric acid and alcohol. The steel structure was studied on thin foils using a μVizo-MET-221 metallographic microvisor (LOMO, Russia), XRD-7000S X-ray diffractometer (Shimadzu, Japan), and EM-125 transmission electron microscope (Russia) [13–16]. The electric discharge machining was used for cutting test foils 150–200 nm thick fabricated by electrolythic thinning on the surface and at 2 mm and 10 mm distances to the surface. The film preparation for TEM study is schematically given in Fig. 1.

The Brinell and Rockwell scales were used to characterize the indentation hardness of the rail running surface in conformity with the Russian specifications. Additionally, the hardness was measured in the upper part of the rail web, approximately 30 mm higher the point 6 of specifications and in the rail head cross-section, at a penetration depth of 2, 10 and 22 mm, along the vertical axis of symmetry. The microhardness measurements were conducted on a PMT-3

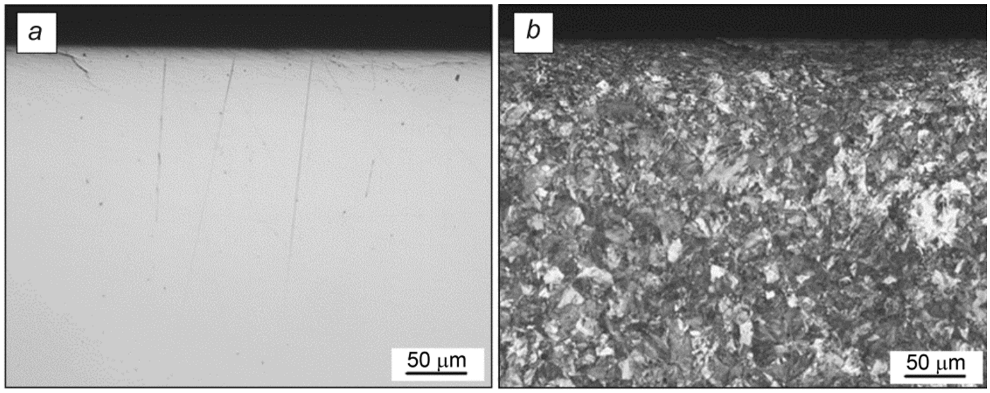

Fig. 2. Rail running surface structure: *a* – nonetched microsection, *b* – etched microsection.

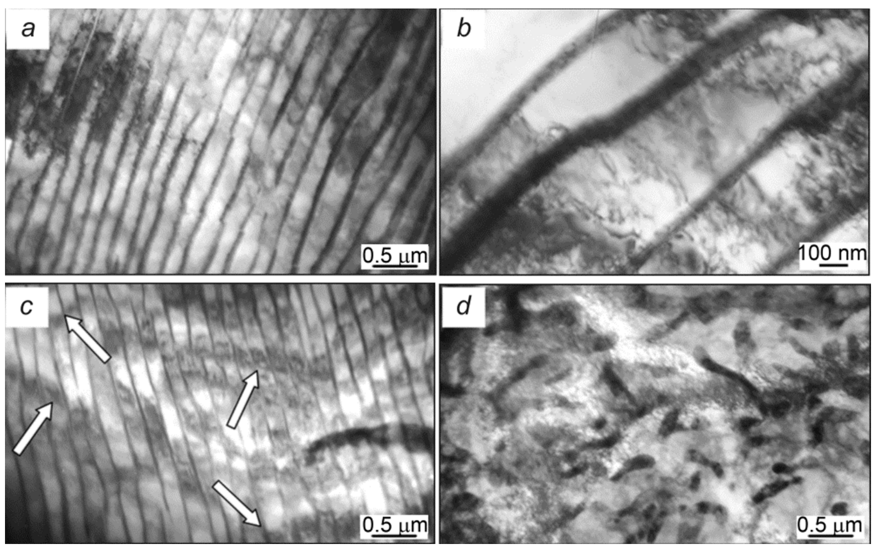

Fig. 3. TEM images of rail steel layer at 10 mm depth from the rail running surface.

Vickers hardness tester (LOMO, Russia) at a 300 mN load of the indenter and 2 mm and 10 mm penetration depths. Microhardness was measured 5 times at each penetration depth.

RESULTS AND DISCUSSION

According to the hardness measurements on the rail head cross-section, the Rockwell C scale hardness (HRC) values are 37.1 at a 2 mm, 35.8 at 10 mm and 35.6 at 22 mm penetration depths. One can see that the hardness level 37.1 HRC at 2 mm penetration depth is higher than at a depth of 10 and 22 mm. This is probably because deep deformation at the center of the material. The microhardness at a 2 mm depth reaches 1481 MPa, whereas at a 10 mm depth, it is 1210 MPa, which is considerably lower. The difference in the microhardness and HRC values can be attributed to the steel structure and phase composition that change during the rail operation.

Nonetched microsections cut from the rail head surface demonstrate slight discontinuances up to 30 μm depth, as presented in Fig. 2*a*. As can be seen from Fig. 2*b*, the surface deformation depth is 35 μm, which is insignificant.

According to TEM observations, the steel layer at a depth of 10 mm contains mostly lamellar perlite. This is shown in Fig. 3*a*. The cementite layers observed in the perlite colonies are curved and separated by ferrite bridges. The

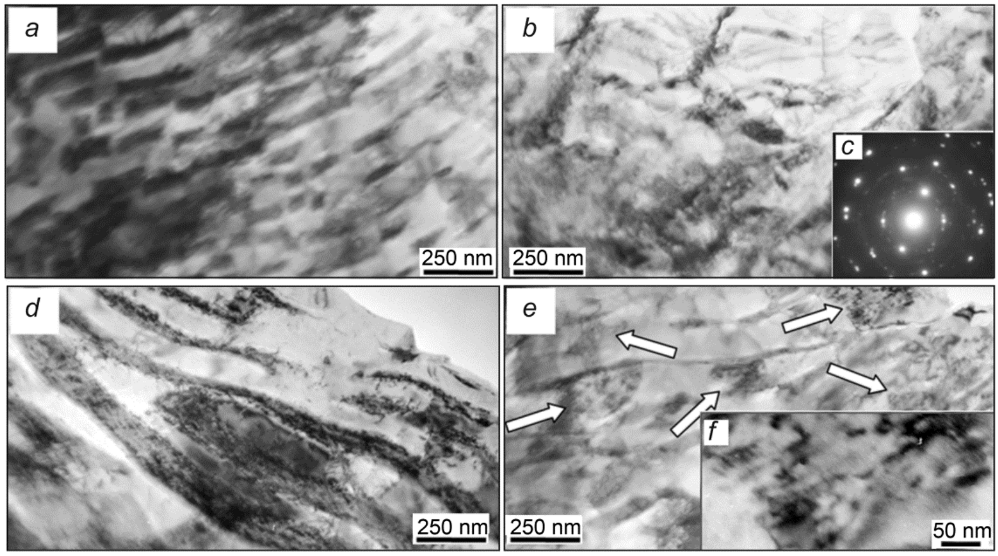

Fig. 4. TEM images of rail running surface structure at 2 mm depth. White arrows indicate bend extinction contours in perlite colonies.

relative content of lamellar perlite is 70% of the steel structure. Ferrite in the perlite colonies manifests a dislocation substructure. Dislocations arrange either chaotically or in aggregations, as presented in Fig. 3*b*. The scalar dislocation density detected on micrographs by the secant method applied at random [17], is $2.54 \cdot 10^{10}$ cm^{-2}.

As shown in Fig. 3*c*, the perlite colonies contain bend extinction contours indicated by white arrows [18]. These bend extinction contours denote the bending and torsion of the material crystal lattice. Using the methodologies utilizing bend extinction contours proposed by Koneva *et al.* [19], we evaluate the excess dislocation density, which causes bending and torsion of the crystal lattice in the foil. It is found that the excess dislocation density at a 10 mm depth of the rail running surface, is $1.7 \cdot 10^{10}$ cm^{-2}. Degenerated pearlite colonies detected in the lower amount (25%) in the structure of the investigated layer, contain globular cementite grains (Fig. 3*d*) and free ferrite grains in the amount of 5 % of the steel structure.

The layer structure at a 2 mm depth from the rail running surface differs from the layer structure at a 10 mm depth. The main difference is the colonies of lamellar perlite comprising the cementite layers that are cut and shifted relative to each other, as presented in Fig. 4*a*. Another difference is shown in Fig. 4*b*, in which the fragmented (subgrain) structure forms in degenerated perlite grains. In Fig. 4*c*, one can see strands in the α-phase allowing to determine the 5-degree azimuthal misorientation angle of the dislocation substructure elements.

The third difference presented in Fig. 4*d*, is the fracture of the cementite layers in the colonies of lamellar perlite due to their dissolution after a transfer of carbon atoms to the dislocations followed by the formation of cementite nanoparticle in the ferrite aggregations. Rounded and, sometimes, lamellar cementite nanoparticles usually locate on the dislocation lines, fixating them and creating a dislocation network, as shown in Fig. 4*e*, *f*. Apparently, the structure modifications discussed above, result from deep plastic deformation of the steel.

The X-ray diffraction (XRD) analysis and TEM observations allow detecting the structure and phase composition of the rail running surface. The plots of typical XRD patterns are given in Fig. 5.

According to the XRD analysis, the major steel phases include the α-Fe solid solution with the body centered cubic crystal lattice and iron carbide (Fe_3C) or cementite with the orthorhombic crystal lattice. The crystal lattice parameter *a* is 0.28693 and 0.28699 nm for the initial α-Fe solid solution and the rail running surface, respectively. The higher parameter of the α-phase crystal lattice can be explained by the higher concentration of carbon atoms in the solid solution. In Fig. 5, one can see that the XRD patterns significantly widen with increasing parameter of the crystal lattice. This is probably because the small size of the scattering grains and their substantial distortions (microscopic stresses). The diffraction peak shape, shifts and widening are therefore analyzed to identify the average size of the

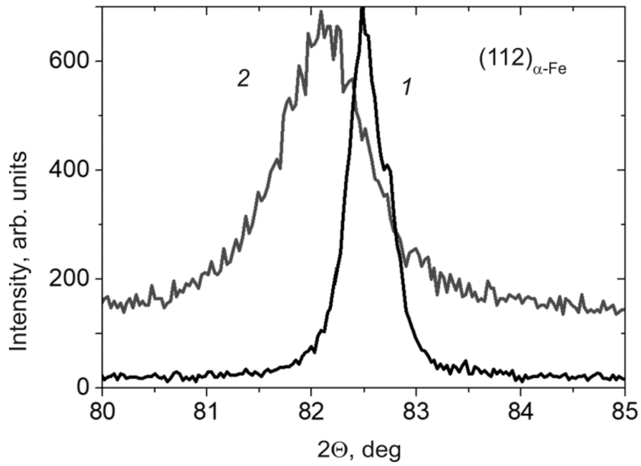

Fig. 5. XRD patterns of α-Fe (112) Bragg reflection: *1* – at 20 mm depth; *2* – rail running surface.

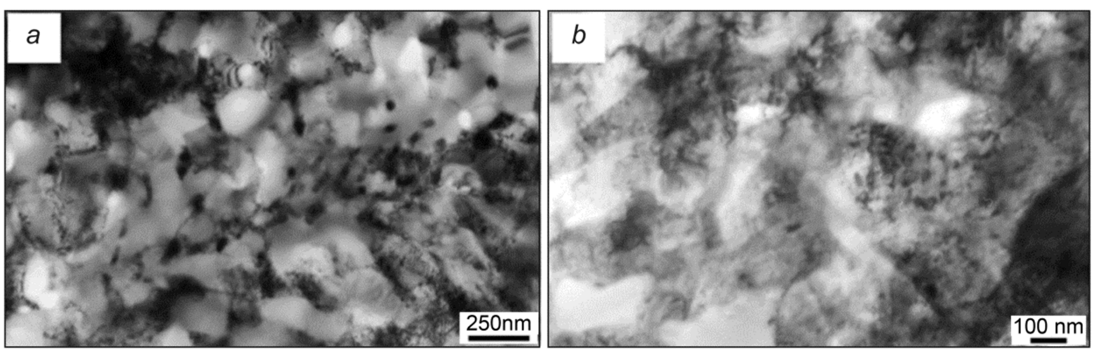

Fig. 6. TEM images of the steel layer structure adjacent to the rail running surface.

coherent scattering region and microdeformations [20]. It should be taken into consideration that if the size D of the coherent scattering region is large and/or the crystal lattice microdistortion ε is low, these parameters cannot be calculated. Therefore, the minimum size D and the maximum microdistortion ε can be obtained from the width of the XRD patterns, *viz*. $0.005\ \mu m < D < 0.2\ \mu m$ and $10^{-4} < \varepsilon < 10^{-2}$. The XRD analysis shows that it is impossible to determine the size of the coherent scattering region and microdistortion $(\Delta d/d)_{ini}$ for the initial steel state. This means that $D_{ini} > 0.2\ \mu m$ and $(\Delta d/d)_{ini} < 10^{-4}$. These parameters are $D = 22.06$ nm and $\Delta d/d = 1.562\cdot10^{-3}$ for the rail running surface. Thus, after the train traffic with the gross rail load of 1411 million tons, the rail running surface is characterized by the small coherent scattering region and comparatively high crystal lattice microdistortion of the α-phase. TEM images of the steel layer structure, which forms the rail running surface, are presented in Fig. 6.

According to Fig. 6, the perlite structure is substantially modified after the extremely long operation time. Along with the lamellar perlite colonies, a 55% relative content of the subgrain structure is detected in the steel surface (Fig. 6*a*). The subgrain size ranges between 100 and 150 nm. Carbide phase particles observed along the subgrain boundaries and at their intersections, have the size varying from 30 to 55 nm. As Fig. 6*b* shows, the second phase particles are often observed in the subgrain volume, on the dislocation lines. Their size ranges from 10 to 15 nm. The scalar dislocation density in the structure of the perlite colonies is $3.7\cdot10^{10}$ cm^{-2}, whereas in the subgrain structure it is $3.0\cdot10^{10}$ cm^{-2}. A comparison of these values with the above findings shows that the scalar dislocation density of the surface layer is 1.5 times higher than that of the layer at a 10 mm depth. The same is observed for the excess dislocation density, which also increases by 1.5 times in the rail running surface.

CONCLUSIONS

This paper has clearly shown that after the train traffic with the gross rail load of 1411 million tons, the hardness levels of the bulk-hardened rails were 37.1, 35.8 and 35.6 HRC at 2 mm, 10 mm and 22 mm depths, respectively. It was suggested that the increase in the hardness level was caused by deep deformation of the rail running surface. According to the XRD analysis, slight discontinuances up to 30 μm depth were detected on the rail cross-sections. The metallographic analysis showed that the deformation depth on the rail running surface was insignificant and did not exceed 35 μm. Investigations performed by using modern techniques of material physics, demonstrated that the extremely long operation conditions resulted in multiple structure transformations of the rail running surface. First, it was the fracture of lamellar perlite and the formation of the submicron size (100–150 nm) subgrain structure in the perlite colonies. Second, the formation of carbide phase particles with the size of the nanometer range was observed on the grain boundaries and in the subgrain volume. Third, the growth in the microdistortions and the crystal lattice parameter was identified in the α-Fe solid solution. Fourth, the occurred steel strain hardening resulted in a 1.5 time increase in the scalar and excess dislocation densities relative to the initial steel state.

This work was financially supported by Grant N 19-32-60001 from the Russian Foundation for Basic Research. The authors thank E. V. Polevoy for providing specimens and valuable discussions.

REFERENCES

1. V. E. Gromov, O. A. Peregudov, and Yu. F. Ivanov, *et al*., Evolution of Structure and Phase Composition of Rail Metal During Long-Term Operation [in Russian], SB RAS, Novosibirsk (2017).
2. Yu. Ivanisenko, Lojkowski W., and R. Z. Valiev, *et al*., Acta Mater., **51**, No. 18, 5555–5570 (2003).
3. W. Lojkowski, M. Djahanbakhsh, G. Bürkle, *et al*., Mat. Sci. Eng. A-Struct., **303**, No. 1–2, 197–208 (2001). DOI: 10.1016/S0921-5093(00)01947-X.
4. Yu. Ivanisenko, I. Maclaren, X. Souvage, *et al*., Acta Mater., **54**, No. 6, 1659–1669 (2006). DOI: 10.1016/j.actamat.2005.11.034.
5. J.-W. Seo, H.-K. Jun, S.-J. Kwon, and D.-H. Lee, Int. J. Fatigue, **83**, 184–194 (2016). DOI: 10.1016/j.ijfatigue.2015.10.012.
6. R. Lewis, P. Christoforou, W. J. Wang, *et al*., Wear, **430–431**, 383–392 (2019). DOI: 10.1016/j.wear.2019.05.030.
7. R. Skrypnyk, M. Ekh, J. C. O. Nielsen, and B. A. Pålsson, Wear, **428–429**, 302–314 (2019). DOI: 10.1016/j.wear.2019.03.019.
8. D. Kim, L. Quagliato, D. Park, and N. Kim, Wear, **420–421**, 184–194 (2019). DOI: 10.1016/j.wear.2018.10.015.
9. Yu. F. Ivanov, O. A. Peregudov, K. V. Morozov, *et al*., IOP Conf. Ser.: Mater. Sci. Eng., **112**, 012038 (2016). DOI: 10.1088/1757-899X/112/1/012038.
10. V. E. Gromov, O. A. Peregudov, Y. F. Ivanov, *et al*., AIP Conf. Proc., **1783**, 020069 (2016).
11. V. E. Gromov, A. A. Yuriev, Yu. F. Ivanov, *et al*., Mater. Lett., **209**, 224–227 (2017). DOI: 10.1016/j.matlet.2017.07.135.
12. A. A. Yur'ev, V. E. Gromov, K. V. Morozov, and O. A. Peregudov, Steel Transl., **47**, 658–661 (2017). DOI: 10.3103/S0967091217100126.
13. F. R. Egerton, Physical Principles of Electron Microscopy. Springer International Publishing, Basel (2016).
14. C. S. S. R. Kumar, ed., Transmission Electron Microscopy. Characterization of Nanomaterials, Springer, New York (2014).
15. C. B. Carter and D. B. Williams, Transmission Electron Microscopy, Springer International Publishing, Berlin (2016).
16. P. B. Hirsch, A. Howie, R. B. Nicholson, *et al*., Electron Microscopy of Thin Crystals [Russian translation], Mir, Moscow (1968).

17. L. M. Utevskii, Diffraction Electron Microscopy in Metal Science [in Russian], Metallurgiya, Moscow (1973).
18. G. Thomas and M. J. Goringe, Transmission Electron Microscopy of Materials [Russian translation], Nauka, Moscow (1983).
19. N. A. Koneva, E. V. Kozlov, L. I. Trishkina, and D. V. Lychagin, in: Proc. Int. Sci. Conf. ‘New Methods in Physics and Deformable Body Mechanics," TSU, Tomsk (1990), pp. 83–93.
20. S. S. Gorelik, Yu. A. Skakov, and L. N. Rastorguev, Radiographic and Electrooptic Analysis [in Russian], MISIS, Moscow (1994).